Hindawi Publishing Corporation
Advances in Materials Science and Engineering
Volume 2014, Article ID 363917, 8 pages
http://dx.doi.org/10.1155/2014/363917

Research Article

NiTi Intermetallic Surface Coatings by Laser Metal Deposition for Improving Wear Properties of Ti-6Al-4V Substrates

Mokgadi Nomsa Mokgalaka,[1,2] Sisa Lesley Pityana,[1,2] Patricia Abimbola Idowu Popoola,[2] and Tebogo Mathebula[1]

[1] *Council of Scientific and Industrial Research, National Laser Centre, Building 46F, P.O. Box 395, Pretoria 0001, South Africa*
[2] *Department of Chemical, Metallurgical and Materials Engineering, Tshwane University of Technology, PMB X680, Pretoria 0001, South Africa*

Correspondence should be addressed to Sisa Lesley Pityana; spityana@csir.co.za
and Patricia Abimbola Idowu Popoola; popoolaapi@tut.ac.za

Received 24 October 2013; Accepted 4 February 2014; Published 17 March 2014

Academic Editor: Feng Zhao

The NiTi intermetallic possesses a number of good properties, such as high wear, oxidation, and corrosion resistance. This paper focuses on the deposition of NiTi intermetallic coatings on Ti6Al4V substrate by laser melting of Ti and Ni elemental powder mixtures. The effect of varying the Ti content in the NiTi composition on the microstructure and wear properties of the coatings was investigated. The microstructure of the NiTi intermetallic coatings were characterized by the scanning electron microscope (SEM) equipped with Energy Dispersive Spectroscope (EDS). The wear properties of the coatings were performed under accelerated dry sliding wear tests. The results obtained from the SEM/EDS analysis; show that the coatings consist of Ni and Ti elements from the feedstock, and the NiTi, $NiTi_2$ and $NiTi_3$, intermetallic phases. Dry sliding wear analysis revealed that there is correlation between the hardness and the wear rate. The coatings displayed significant improvement in wear resistance up to 80% compared to the substrate.

1. Introduction

Titanium alloys have low hardness values, poor resistance to wear, and oxidation at high temperatures [1]. These limitations can be overcome by changing the nature of the surface of titanium alloys using different surface engineering techniques. Methods such as nitriding, thermal spraying, and chemical or physical vapour deposition (CVD or PVD) have been well-known technologies that improve the surface properties of titanium and titanium alloys. However, these methods have limitations such as a long processing time, easy deformation, and limited bond strength between the coating and the substrate [2]. Laser processing techniques have been found to be free from these shortcomings and can be used to enhance the surface properties of ferrous and nonferrous metal surfaces [3–6].

As a flexible process, laser processing can be used in the deposition of different coatings either to improve the surface properties or to refurbish worn-out parts [7]. Amongst the many benefits of the laser surface coating methods, laser deposition is the preferred method because of the novel microstructures and phases that can be formed due to rapid cooling and solidification rates associated with the processing technique [8]. Coatings generally have such microstructures that cannot be easily obtained by conventional techniques. One of the advantages of laser surface coating is that quite a number of metallic powders can be used to form intermetallic compounds exhibiting excellent wear resistance, good corrosion, and oxidation properties.

The Ti-Ni coatings have been a subject of great interest and have been widely exploited for a range of applications including aerospace, biomedical engineering, and microelectrochemical system due the above-mentioned advantageous properties [9–13]. Stainless steel surfaces were coated with NiTi to enhance mechanical properties and corrosion resistance using different deposition techniques, including plasma

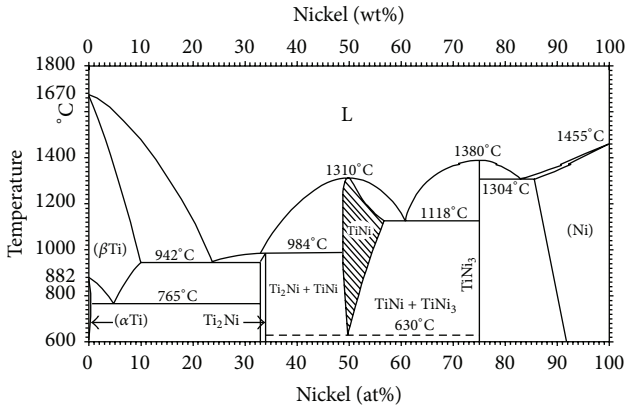

Figure 1: Equilibrium Ni-Ti phase diagram [20].

Table 1: Chemical composition of titanium alloy Ti6Al4V.

Element	Al	V	C	Fe	Cr	N	O	Ti
wt.%	6.11	4.17	0.083	0.083	0.001	0.014	0.02	Bal.

Table 2: Experimental process parameters for depositing the NiTi intermetallic coatings.

Sample	Process parameter	Values
Ti50Ni50	Laser power	800 W
	Beam spot diameter	2 mm
Ti55Ni45	Scanning speed	8 mm/s
	Powder feed rate	3 g/min
Ti45Ni55	Gas shielding and carrier	Argon
	Gas flow rate	5 L/min

transfer arc (PTA), plasma welding, plasma spray coating, and sputtering process, all with different degrees of success [14–17].

Ozel et al. [18] studied microstructure characteristic of NiTi coating on stainless steel by transferred arc process. When the arc current was at 90–100 A, the amount of NiTi phase decreased and high dilution was observed. The coatings produced had a magnitude between 1 and 1.4 mm with the highest hardness values between 500 and 550 HVN. Van der Eijk et al. [19] studied plasma welding of NiTi to NiTi, stainless steel, and Hastelloy C276. The microstructure produced as a result of welding NiTi to NiTi had defects such as cracking, Ti carbides, and high volume of $NiTi_2$ phase. The strength of the weld was found to be less than that of the base material. Microstructure produced from the NiTi stainless steel weld had large cracks propagating from the NiTi side of the weld. This was attributed to the amount of NiTi melting larger than stainless steel which results in absorption of elements from the steel into NiTi.

The Ti-Ni binary phase diagram is shown in Figure 1 [20]. It indicates that this system contains the stable NiTi, Ni_3Ti, and $NiTi_2$ phases. The good toughness and ductility and the exhibited NiTi phase make it an ideal candidate for wear resistant application. The Ti_2Ni and Ni_3Ti are regarded as suitable particles for metal matrix reinforcements.

In this study, mechanically alloyed Ti and Ni elemental powders will be used to form *in situ* NiTi intermetallic thin surface coatings on the Ti6Al4V substrate. The laser metal deposition technique will be employed to melt powders of different compositions: Ti50Ni50, Ti45Ni55, and Ti55Ni45. The microstructure, phase composition, and microhardness of the coatings will be investigated.

2. Experimental Procedure

2.1. Materials. The materials used in the experiment are elemental nickel and titanium powders with the particle size fraction within the range of +45 microns and −63 microns. Prior to milling, the powders were weighed and mixed together to give nominal compositions of Ti55Ni45, Ti50Ni50, and Ti45Ni55 in weight%. The initially mixed powders were mechanically alloyed in a planetary ball mill by subjecting the particles to repeated welding, fracturing, and rewelding from the collision of the particles and the grinding medium. The milling was performed for two hours to allow the powders to reach a steady state where homogeneous NiTi powder was produced. The ball to powder ratio was kept uniform at 10 : 1 and the rotation speed of 300 rpm. After milling, the powder mixture was analysed by scanning electron microscopy to determine the change in morphology and the particle size.

2.2. Laser Surface Coating. The substrate material used was Ti6Al4V plate, with $72 \times 72 \times 5\,mm^3$ dimensions. The plates were sandblasted and cleaned with acetone prior to the laser coating process. Table 1 shows the chemical composition of the titanium alloy Ti6Al4V. The NiTi prealloyed powders were free flowing. The powders were fed through a three-way nozzle with argon shielding gas stream. The argon gas flow rate was 5 L/min. The laser deposition process was carried out using a CW 4.4 kW Rofin Sinar Nd:YAG laser operating with 1.064 μm wavelength. The beam spot on the target was 2 mm in diameter. The scanning speed, laser power, and the powder flow rate were kept constant. Table 2 shows the experimental parameters used for depositing the NiTi intermetallic coatings.

2.3. Materials Characterization. Metallographic samples were sectioned with a Corundum L205 cut-off wheel using a Struers Discotom-2 cutting machine. After sectioning, the specimens were hot mounted in clear thermosetting Bakelite resin. The specimens were then ground and polished to a 0.04-micron (OP-S suspension) surface finish with a Struers TegraForce-5 auto/manual polisher and etched in Kroll's reagent by immersing the samples for approximately 10 seconds. Microstructure was characterized on OlympusBX51 M Optical Microscope (OM) and Jeol JSM 6510 Scanning Electron microscopy (SEM) built with Energy Dispersive Spectroscopy (EDS). X-ray diffraction (XRD) was conducted using the Rigaku/Dmax 2200 pc automatic X-ray diffractometer with Cu target Ka radiation to identify the phase constitution.

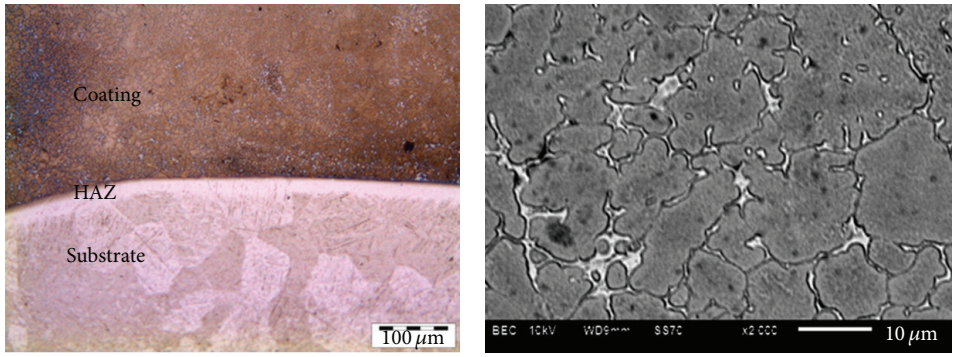

(a) (b)

Figure 2: Micrographs of the laser deposited Ti50Ni50 coating; (a) optical image showing the interface of the coating and substrate; (b) SEM image of the coating.

3. Results and Discussion

3.1. Microstructural and X-Ray Diffraction Analysis

3.1.1. Ti50Ni50 Coating. As the Ni and Ti powder particles were scanned by the laser beam along with the substrate, the molten particles reacted with each other and with substrate forming a melt pool. The melt pool rapidly solidified as the laser beam was moved across the substrate forming a clad track on the titanium substrate. Due to the rapid nonequilibrium solidification, the NiTi intermetallic compounds precipitated on the substrate. The possible exothermic chemical reactions and products of the powders are [21]

$$\begin{aligned} \mathrm{Ti} + \mathrm{Ni} &\Longrightarrow \mathrm{TiNi} + 67\ \mathrm{KJ/mol} \\ 2\mathrm{Ti} + \mathrm{Ni} &\Longrightarrow \mathrm{Ti_2Ni} + 83\ \mathrm{KJ/mol} \\ \mathrm{Ti} + 3\mathrm{Ni} &\Longrightarrow \mathrm{TiNi_3} + 140\ \mathrm{KJ/mol} \end{aligned} \quad (1)$$

The microstructural images of the cross section of the deposited coatings were taken at different places of interest on the coating to understand the morphology of the microstructure and the distribution of nickel-titanium within the coating. Typical optical and SEM micrographs of the laser deposited coatings are shown in Figure 2.

Figure 2(a) shows the cross section of the laser deposited Ti50Ni50 coating on the Ti6Al4V substrate with a thickness of 550 μm and dilution rate of 6.3%. There were no cracks or pores observed within the coating, and most significantly good bonding between the substrate and the coating was achieved. SEM image of the coating showing distribution of the phases is presented in Figure 2(b). The contrast of the image indicates the presence of different phases. Elemental analysis performed on the coating revealed that the grey structures are a matrix consisting of TiNi phase and the light phases around the grain boundaries are $TiNi_2$ and $TiNi_3$ phases.

XRD results recorded for the Ti50Ni50 coating, in the range 2θ from 20° to 90°, are shown in Figure 3. There are four intermetallic phases identified in the coating, martensite NiTi (B19′), austenite NiTi (B2), $NiTi_2$, and Ni_3Ti, together with the main peaks of Ti. The elemental Ni peaks were not observed indicating that the Ni and Ti powders reacted with each other to form *in situ* Ni-Ti intermetallic phases. The existence of the Ti peaks is attributed to the abundance of Ti as the substrate and the added Ti powder. The main peaks for the NiTi (B19′) phase occur at 2θ = (38.25°, 39.49°, 41.85°, 44.0°, and 45.2°). A broad peak at 2θ = 42.7° is identified as the NiTi (B2) phase. The Ti-rich $NiTi_2$ phase occurs at 2θ = (45.7°, 70.98°, 72.18°, 76.63°, 77.65°, and 85.65°). The Ni-rich $TiNi_3$ phase has weak peaks at 2θ = (43.7° and 52.96°). The Ti peaks occur at 2θ = (35°, 38°, 40°, and 63.44°). Some traces of TiO_2 were detected at 2θ = 27.96°. The volume of the martensite to austenite content in the coating could not be determined from the XRD data.

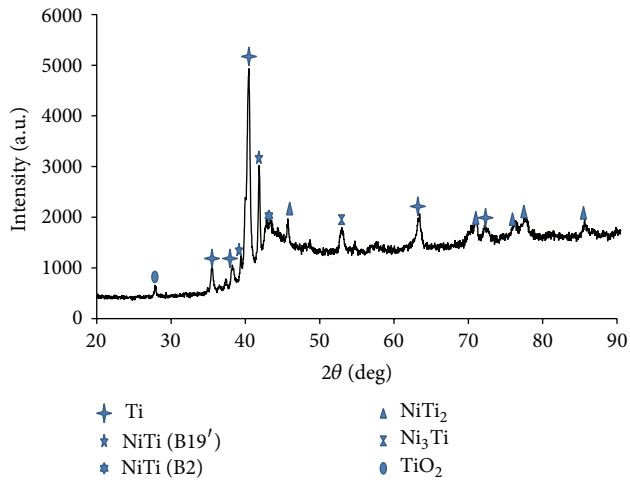

Figure 3: XRD patterns of Ti50Ni50 coating.

3.1.2. Ti55Ni45 Coating. Ti55Ni45 coatings deposited from processing parameters similarly as in the previous case are presented in Figure 4. Coatings with a layer thickness of 500 μm and dilution rate of 6.9% were obtained. The sample was slightly overetched in order to enhance the grain boundaries. Figure 4(a) shows the optical micrographs of the coating comprised of three phases, brown structures surrounded

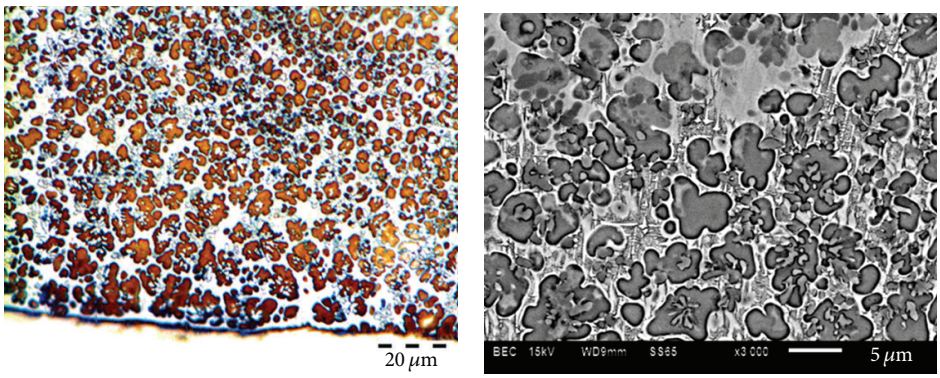

(a) (b)

Figure 4: Micrographs of the laser deposited Ti55Ni45 coating; (a) optical image indicating different phases within the coating; (b) SEM image showing high magnification of the coating.

by bright/white structures and white phase occurring at the centre of the brown structures. The brown structures were identified as TiNi phase, with the bright/white identified as Ti_2Ni, while the white structures occurring mostly at the centre of the TiNi phase were identified as the Ti phase. It is observed that the Ti-rich phase occurs with two different morphologies, flower-like structures and spherical-like structures uniformly distributed within the coating. The occurrence of this phase in two morphologies was attributed to the excess Ti that did not react with the molten Ni causing it to remelt on its own forming Ti particles, while the flower-like structures are the titanium that fully reacted with nickel forming NiTi intermetallics. High magnification of SEM image of the coating is revealed in Figure 4(b) showing uniform distribution of the phases that formed during melting.

The XRD phase analysis of the Ti55Ni45 coating is presented in Figure 5; the results indicate that the coating consists of the NiTi (B19′) martensite and NiTi (B2′) austenite phases in accordance with the OM and SEM micrographs. The $NiTi_2$ phase is also detected along with the pure Ti peaks. For this coating no Ni-rich phases were detected by the XRD. The overall major peaks are NiTi martensite B19 and austenite B2, $NiTi_2$, and Ti as it is in abundance. There are no Ni_3Ti, Ni_4Ti_3, and TiO_2 traces observed as seen with other compositions.

3.1.3. Ti45Ni55 Coating. Optical micrograph and SEM image of the laser deposited Ni55Ti45 coating with a thickness of 550 μm and dilution rate of 6.5% are presented in Figure 6. The microstructure revealed good homogeneity and uniformity with equiaxed grains and a dendritic structure. The coating consists of dark brown structures reported to be NiTi and light white structures with a flower-like morphology identified as Ti-rich phase as observed in Figure 6(a). The light white structure occurring between the NiTi phases observed previously is also present; however, in this coating they appear as interconnected matrix throughout the coating. Figure 6(b) shows a SEM image at a high magnification indicating the interconnected matrix in the coating.

Figure 7 reports the XRD results recorded for the Ti45Ni55 laser coating in the 2θ range from 20° to 80°. Three

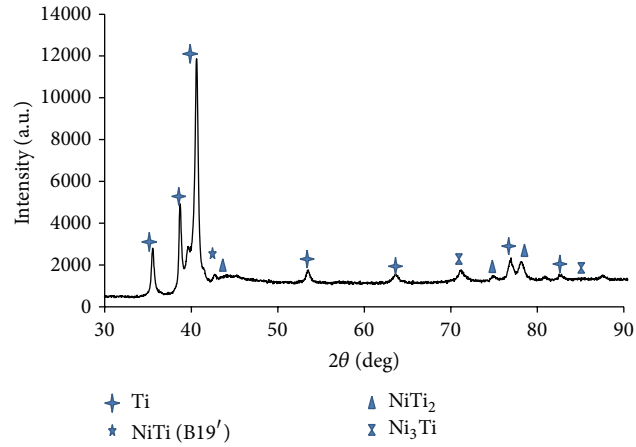

Figure 5: XRD patterns of Ti55Ni45 coating.

intermetallic phases NiTi austenite, $NiTi_2$, and Ni_3Ti were identified in the coating. The occurrence of the Ti peaks in abundance was attributed to the Ti6Al4V substrate that is used and the added Ti powder as seen in the previous results. Major peaks observed were Ni_3Ti and $NiTi_2$ with Ti overlapping each other at some peaks. Few peaks of Ni_3Ti phase occur at 2θ = (42.74°, 47.94°, and 82.97°). Weak peaks of $NiTi_2$ which overlapped with some Ti peaks occur at 2θ = (38.78°, 53.61°, 71.26°, and 77.06°), while Ti phase is occurring at 2θ = (36.62°, 38.78°, 40.67°, 53.61°, 63.7°, 71.26°, and 77.06°). NiTi austenite phase has weak peak at 2θ = (42.74°) and martensite phase was not observed, but some traces of TiO_2 were observed at 2θ = (44.08°).

3.2. Microhardness Analysis. Hardness profile across the depth of the NiTi metallic coating was measured by the Matsuzawa Seiki hardness tester at a load of 100 g, spacing of 50 μm, and dwell time of 15 seconds. Hardness profile of the deposited NiTi showing the hardness values in the coating, heat affected zone, and the substrate is presented in Figure 8. Experimental results indicate that the surface hardness of the laser deposited NiTi coatings had an increased hardness value compared to the parent material Ti-6Al-4V alloy. High

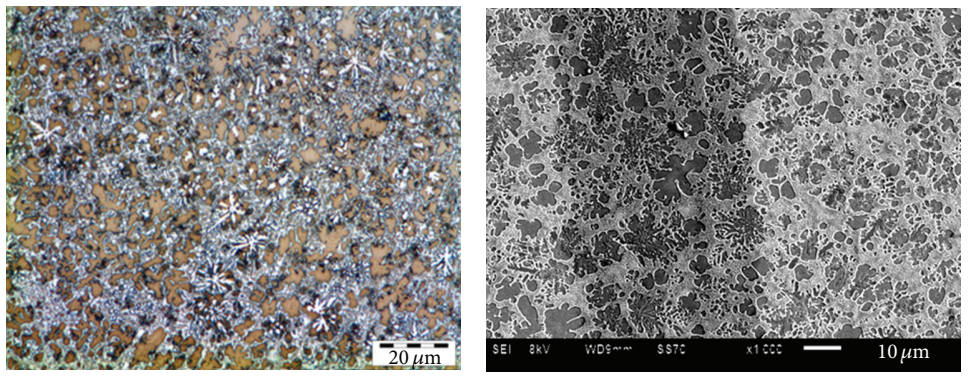

(a) (b)

Figure 6: Micrographs of the laser deposited Ti45Ni55 coating; (a) optical image showing distribution of the phase in the coating; (b) SEM image showing a high magnification of the coating.

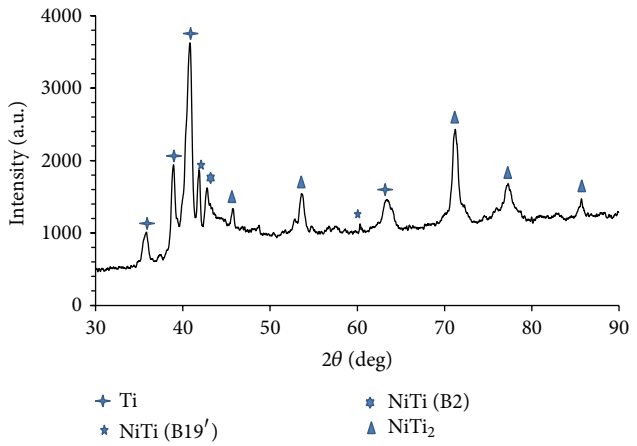

Figure 7: XRD patterns of Ti45Ni55 coating.

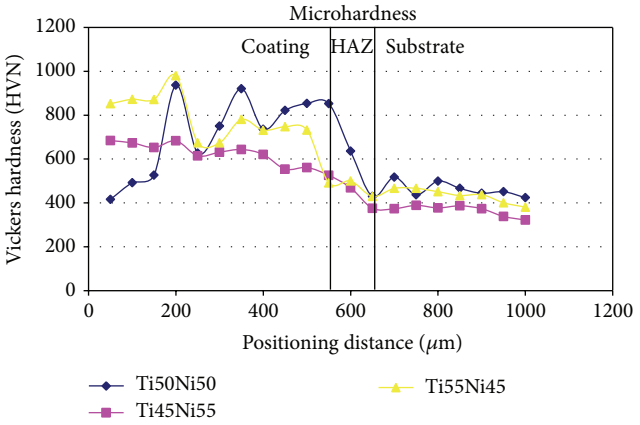

Figure 8: Microhardness measurement of laser deposited coatings.

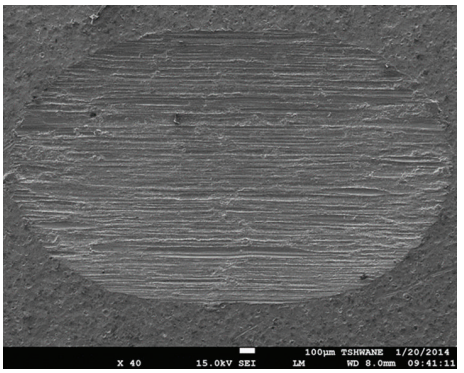

(a)

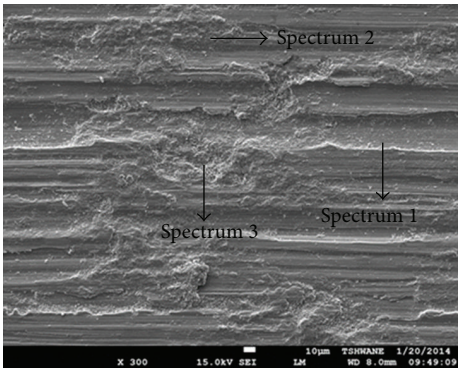

Element (wt.%)	C	N	O	Al	Ti	V
Spectrum 1	2.63	–	–	7.51	88.44	1.42
Spectrum 2	1.60	1.01	14.34	3.26	75.37	3.15
Spectrum 3	3.52	1.83	28.82	4.73	58.86	2.24

(b)

Figure 9: Wear track of the Ti-6A1-4V substrate after sliding against a tungsten carbide ball.

hardness in the deposited layer is attributed to the formation of the fine grained microstructure produced during melting and formation of the hard intermetallic phases. The Ti55Ni45 coating had high hardness values compared to Ti45Ni55 and Ti50Ni50 coatings with the average value of 430 HV higher than that of Ti-6Al-4V (380 HV) substrate. The high hardness displayed by the coating (742 HV) is a result of excessive amount of Ti elemental powder that was well dispersed within the coating resulting in increased volume of inert

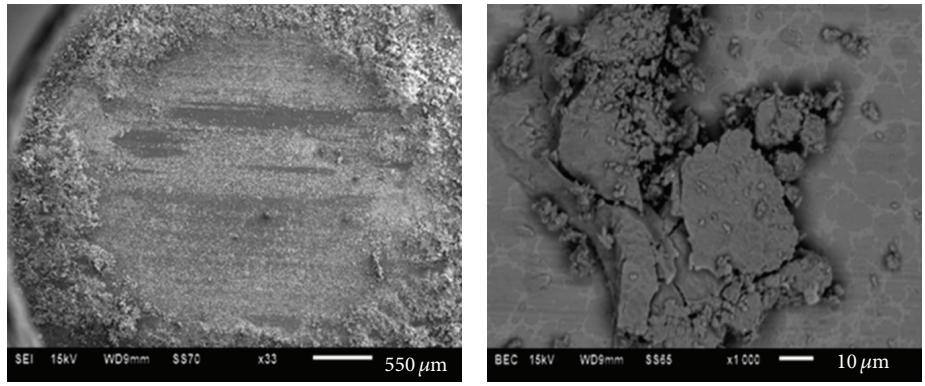

(a) (b)

Figure 10: Wear track of the laser deposited Ni50Ti50 after sliding against a tungsten carbide ball.

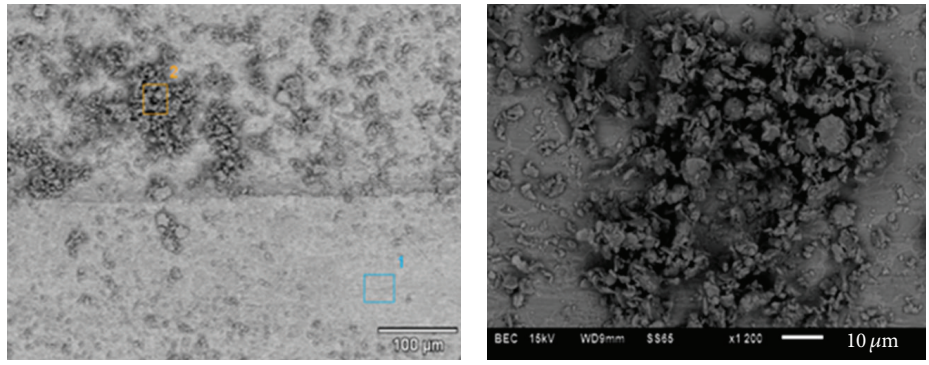

(a) (b)

Figure 11: Wear track of the laser deposited Ni55Ti45 after sliding against a tungsten carbide ball.

secondary phase $NiTi_2$ known for high hardness but with brittle microstructure.

3.3. Wear Measurement. The deposited NiTi coatings were subjected to wear testing using a tungsten carbide (WC) ball at a load of 20 N for 17 minutes. Figure 9(a) displays the wear track of the Ti-6Al-4V substrate subjected to abrasive wear. The examined worn surface presented in Figure 9(b) indicated the presence of wear debris, large pits, and deep grooves on the surface of the material. Severe degree of plastic deformation was evident on the worn surface demonstrating that the mechanism is adhesion and abrasive wear.

The wear track of the laser deposited Ti50Ni50 coating is presented in Figure 10(a), showing ploughing mechanism experienced by the coating. Wear debris that detached from the surface stuck together forming cluster that rewelded to the surface of the coating. Alternatively, these clusters remain trapped between the sliding surfaces and spread onto wear track forming an oxide layer presented in Figure 10(b). Plastic deformation and shallow plough grooves on the worn surface of the NiTi show that the coating suffers from nonsevere abrasive and adhesive wear from the hard tungsten carbide ball.

Figure 11(a) displays the wear track of the laser deposited Ni55Ti45 after sliding against a tungsten carbide ball for 17 minutes under dry conditions. It was observed that the wear debris formed consists of loose powder particles that were not compact with the surface of the coating as observed in Figure 11(b). Elemental analysis taken from wear debris demonstrates that the debris formed are a mixture of oxides from oxidation during wear and processing, carbon from the tungsten carbide ball, and nickel-titanium from the surface of the coating. The wear debris were smeared on the tribolayer and further oxidised due to effect of friction and mechanical cavitation as a result of contact between the ball and surface during sliding.

The SEM images of the laser deposited Ni45Ti55 coating after wear tests are presented Figure 12. It can be observed from Figure 12(a) that the debris formed in the coating are in small quantity compared to the coatings fabricated with a composition of Ni50Ti50 and Ni55Ti45. As a result of high content of Ti in the Ni45Ti55, an increased volume of Ti dendrite phase is produced. The Ti dendrites with a hard phase effectively carry the load, because they are formed *in situ*. The interfacial bonding between the NiTi matrix and the Ti dendrites tends to be stronger, and hence the clad layers exhibit better wear resistance than the other coatings. However, cracks expansion on the oxide layer which is believed to be the brittle $NiTi_2$ phase was observed in Figure 12(b). The formation of oxide layer and subsequent

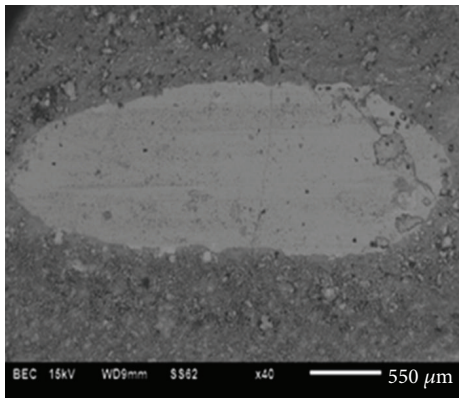

(a)

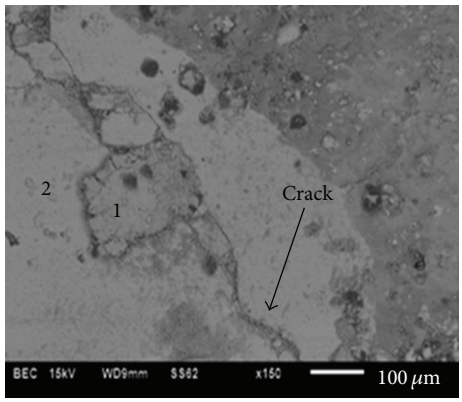

Element (wt.%)	Ti	Ni	Al	C	O	N
Area 1	58.00	16.60	2.22	4.88	12.09	3.78
Area 2	73.85	20.57	1.61	1.64	0.00	0.00

(b)

Figure 12: Wear track of the laser deposited Ni45Ti55 after sliding against a tungsten carbide ball under dry conditions.

compacting as a solid lubricant have been reported to cause a transition from a more to a less severe wear. The results obtained in the analysis of the wear track and the debris from the three coatings are almost the same, and hence it can be concluded that the dominant wear mechanisms (oxidation and abrasive) are the same in all coatings. In comparison with Ti6Al4V alloy, the deposited NiTi coatings presented less degree of deformation. Their worn surfaces clearly signify better wear resistance under dry sliding conditions and room temperature.

From the results obtained in graph presented in Figure 13, low wear rate is notable in coatings fabricated from the Ti55Ni45 composition; these are attributed to the high hardness values and the NiTi (B2), $NiTi_2$, and Ti phases formed during processing. NiTi B2′ experience elastic deformation stress induced martensitic transformation leading to pseudoplastic effect which is accommodated deformation during wear; hence less wear is experienced by the coating. These were not achievable in Ti50Ni50 coating as a result of the high volume of NiTi (B19′). The Ti45Ni55 presented

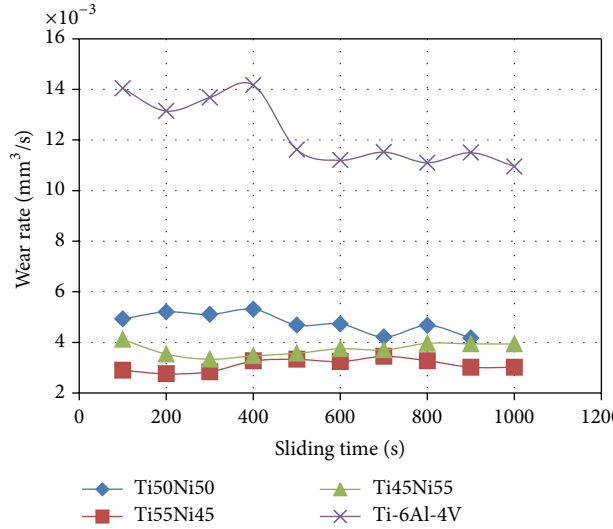

Figure 13: Wear rate analysis of laser deposited coating.

better wear rate compared to the former due to presence of B2 and an increased volume of $NiTi_2$ phase. These is a result of the combination of intermetallic properties of $NiTi_2$ (high hardness and good ductility) and excellent ductility and toughness of NiTi.

4. Conclusions

Surface modification of Ti6Al4 was successfully achieved by fabricating NiTi coatings using laser metal deposition. The coatings produced were metallurgically bonded to the surface without defects such as pores and cracks with minimal dilution between the substrate and the coating. The microstructure of NiTi/Ti6AlV4 coating produced consisted of intermetallic TiNi-$NiTi_2$ alloy. The highest hardness value 742 HV was displayed by Ti55Ni45 coating, with an average value of 430 HV higher than that of Ti6Al4V (380 HV) substrate. The wear resistance was significantly improved with more than five orders of magnitude than that of the substrate. Enhancement of the wear resistance of the coating was achieved as a result of the combination of high hardness, excellent ductility, and toughness exhibited by NiTi. Wear mechanism of the NiTi coating under dry sliding condition is governed by nonsevere abrasive and adhesive wear. Ti dendrites formed during solidification played a major role in improving the properties of the coating as it acted as the reinforcement, strengthening the deposited coating.

Conflict of Interests

The authors declare that there is no conflict of interests regarding the publication of this paper.

Acknowledgments

This material is based on work supported financially by the National Research Foundation. The National Laser Centre,

CSIR, Pretoria, is appreciated for laser facility and financial support. Appreciation goes to Tshwane University of Technology and Mr. Lucas Mokwena.

References

[1] J. J. Polmear, "Titanium alloys," in *Light Alloys*, Edward Arnold, London, UK, 1981.

[2] Y. S. Tian, C. Z. Chen, D. Y. Wang, and T. Q. Lei, "Laser surface modification of titanium alloys—a review," *Surface Review and Letters*, vol. 12, no. 1, article 123, 2005.

[3] M. J. Dutta and I. Manna, "Laser material processing," *International Materials Reviews*, vol. 56, no. 5-6, pp. 341–388, 2011.

[4] J. J. Dai and S. Q. Hou, "Laser gas nitriding of titanium and titanium alloys," *Surface Review and Letters*, vol. 16, no. 6, pp. 789–796, 2009.

[5] A. P. I. Popoola, S. L. Pityana, and O. M. Popoola, "Laser deposition of (Cu + Mo) alloying reinforcements on AA1200 substrate for corrosion improvement," *International Journal of Electrochemical Science*, vol. 6, no. 10, pp. 5038–5051, 2011.

[6] M. Rakhes, E. Koroleva, and Z. Liu, "Improvement of corrosion performance of HVOF MMC coatings by laser surface treatment," *Surface Engineering*, vol. 27, no. 10, pp. 729–733, 2011.

[7] Y. Sun and M. Hao, "Statistical analysis and optimization of process parameters in Ti6Al4V laser cladding using Nd:YAG laser," *Optics and Lasers in Engineering*, vol. 50, no. 7, pp. 985–995, 2012.

[8] E. Yoyserkani, A. Khajerour, and S. Corbin, *Laser Cladding*, CRC Press, Washington, DC, USA, 2005.

[9] S. Sun, Y. Durandet, and M. Brandt, "Parametric investigation of pulsed Nd:YAG laser cladding of stellite 6 on stainless steel," *Surface and Coatings Technology*, vol. 194, no. 2-3, pp. 225–231, 2005.

[10] U. K. Mudali, R. Kaul, S. Ningshen et al., "Influence of laser surface alloying with chromium and nickel on corrosion resistance of type 3041 stainless steel," *Materials Science and Technology*, vol. 22, no. 10, pp. 1185–1192, 2006.

[11] H. Hiraga, T. Inoue, H. Shimura, and A. Matsunawa, "Cavitation erosion mechanism of NiTi coatings made by laser plasma hybrid spraying," *Wear*, vol. 231, no. 2, pp. 272–278, 1999.

[12] M. Salehi, F. Karimzadeh, and A. Tahvilian, "Formation of Ti-Ni intermetallic coatings on carbon tool steel by a duplex process," *Surface and Coatings Technology*, vol. 148, no. 1, pp. 55–60, 2001.

[13] K. Allafi, X. Ren, and G. Eggeler, "The mechanism of multistage martensitic transformations in aged Ni-rich NiTi shape memory alloys," *Acta Materialia*, vol. 50, no. 4, pp. 793–803, 2002.

[14] J. C. Schauer and J. Winter, "Plasma deposition of elastic wear resistant Si-C coatings on nickel-titanium for biomedical applications," *Journal of Applied Physics*, vol. 103, no. 11, Article ID 113302, 2008.

[15] L. Gerke, J. Stella, J. C. Schauer, M. Pohl, and J. Winter, "Cavitation erosion resistance of a-C:H coatings produced by PECVD on stainless steel and NiTi substrates," *Surface and Coatings Technology*, vol. 204, no. 21-22, pp. 3418–3424, 2010.

[16] T. Abubakar, M. Rahman, D. P. Dowling, J. Stokes, and M. S. J. Hashmi, "Adhesion performance of TiN coating with amorphous NiTi alloy interlayer onto 316L stainless biosteel deposited by sputtering process," *Surface Engineering*, vol. 26, no. 7, pp. 499–505, 2010.

[17] M. Bram, A. Ahmad-Khanlou, H. P. Buchkremer, and D. Stöver, "Vacuum plasma spraying of NiTi protection layers," *Materials Letters*, vol. 57, no. 3, pp. 647–651, 2002.

[18] S. Ozel, B. Kurt, I. Somunkiran, and N. Orhan, "Microstructural characteristic of NiTi coating on stainless steel by plasma transferred arc process," *Surface and Coatings Technology*, vol. 202, no. 15, pp. 3633–3637, 2008.

[19] C. van der Eijk, H. Fostervoll, Z. K. Sallom, and O. M. Akselsen, "Plasma welding of NiTi to NiTi, stainless steel and hastelloy C276," in *Proceedings of the ASM Materials Solutions Conference*, pp. 125–129, Pittsburgh, Pa, USA, 2003.

[20] T. B. Massalski, H. Okamoto, P. R. Subramanian, and L. Kacprzak, *Binary Alloy Phase Diagrams*, vol. 3, ASM International, Materials Park, Ohio, USA, 2nd edition, 1990.

[21] C. Zhang, Y. Yang, and W. Xu, "*In situ* synthesis of titanium-nickel intermetallic compounds layer and TiN coating by laser cladding," *OME Information*, no. 5, pp. 33–39, 2006.